Mitochondrial citrate accumulation triggers senescence of alveolar epithelial cells contributing to pulmonary fibrosis in mice

Jie-Ru Hong [a,1], Ling Jin [a,1], Chen-Yu Zhang [a], Wen-Jing Zhong [a], Hui-Hui Yang [a], Guan-Ming Wang [a], Sheng-Chao Ma [b,c], Cha-Xiang Guan [a], Qing Li [d,**], Yong Zhou [a,*]

[a] Department of Physiology, School of Basic Medical Science, Central South University, Changsha, Hunan 410078, China
[b] NHC Key Laboratory of Metabolic Cardiovascular Diseases Research, Ningxia Medical University, Yinchuan 750004, China
[c] The School of Basic Medical Sciences, Ningxia Medical University Yinchuan 750004, China
[d] Department of Physiology, Hunan University of Medicine, Huaihua, Hunan 418000, China

ABSTRACT

Alveolar epithelial cell (AEC) senescence is implicated in the pathogenesis of pulmonary fibrosis (PF). However, the exact mechanism underlying AEC senescence during PF remains poorly understood. Here, we reported an unrecognized mechanism for AEC senescence during PF. We found that, in bleomycin (BLM)-induced PF mice, the expressions of isocitrate dehydrogenase 3α (Idh3α) and citrate carrier (CIC) were significantly down-regulated in the lungs, which could result in mitochondria citrate (citrate^{mt}) accumulation in our previous study. Notably, the down-regulation of Idh3α and CIC was related to senescence. The mice with AECs-specific Idh3α and CIC deficiency by adenoviral vector exhibited spontaneous PF and senescence in the lungs. *In vitro*, co-inhibition of Idh3α and CIC with shRNA or inhibitors triggered the senescence of AECs, indicating that accumulated citrate^{mt} triggers AEC senescence. Mechanistically, citrate^{mt} accumulation impaired the mitochondrial biogenesis of AECs. In addition, the senescence-associated secretory phenotype from senescent AECs induced by citrate^{mt} accumulation activated the proliferation and transdifferentiation of NIH3T3 fibroblasts into myofibroblasts. In conclusion, we show that citrate^{mt} accumulation would be a novel target for protection against PF that involves senescence.

1. Introduction

Pulmonary Fibrosis (PF), a persistent, progressive, and age-related interstitial lung illness of unknown causes [1], is marked by a steady increase in breathlessness, diffuse cellular infiltrates, restrictive lung dysfunction, and impaired gas exchange [2]. Unfortunately, there is no cure for PF yet. Only pirfenidone [3] and nintedanib [4] have been known to reduce the rate of lung function decline, but they are unable to restore the progression or decrease mortality [5]. Therefore, it is essential to explore the molecular components that give rise to the pathogenesis of PF.

As PF is most commonly seen in older men, with a median survival of only 3.8 years after diagnosis in those over 65 years old [6],

age is the most significant risk factor for this condition [7]. Cellular senescence, a state of permanent cell growth arrest, is thought to play a role in the pathogenesis of PF [8]. In mice, removing senescent cells using senolytics, such as dasatinib and quercetin, has been shown to attenuate bleomycin-induced PF [8]. Senescence is characterized by epigenetic abnormalities, telomere damage, DNA damage, and mitochondrial dysfunction, all of which are present in PF [9]. At the cellular level, there is considerable overlap between senescence and PF pathology [10]. Recent research has suggested that accelerated or aggravated alveolar epithelial cell (AEC) senescence is a critical mechanism in the initiation and progression of PF [11]. Induction of senescence in AECs drives PF [12]. Consequently, targeting AEC senescence is an attractive approach for preventing and treating PF. However, the molecular mechanism that triggers AEC senescence during PF is not fully understood.

Recent years have seen a surge of interest in the role of glucose metabolic reprogramming in cell senescence [13]. Warburg effect, a well-documented form of glucose metabolism reprogramming in tumor tissue, is a prime example [14]. Metabolites and intermediates of glucose metabolic reprogramming, such as hexokinase 2 [15] and pyruvate [16], have been identified as key signaling molecules in the process of cellular senescence. Citrate is mainly synthesized in the mitochondria from pyruvate, a product of glucose metabolism. Isocitrate dehydrogenase 3 (IDH3) catalyzes the transformation of citrate into α-ketoglutaric acid [17]. Additionally, citrate is transported from the mitochondria to the cytoplasm by citrate carrier (CIC, encoded by Slc25a1) and then broken down into acetyl-CoA and oxalacetic acid by ATP-dependent ATP citrate lyase (ACLY) [17]. Citrate has been found to be a crucial signaling molecule in cellular senescence and related diseases [18,19]. It has been observed that citrate can induce disruption of lipid metabolism in tumor cells, leading to tumor cell senescence and growth inhibition [20]. Moreover, inhibition of IDH1 has been demonstrated to induce cell senescence and inhibit tumor cell proliferation in highly malignant ovarian cancer cells [21]. In addition, our previous research has revealed that mitochondrial citrate (citrate^{mt}) accumulation can worsen necroptosis of AECs and consequently aggravate acute lung injury (ALI) in mice [22]. However, the role of citrate^{mt} in the senescence of AECs and PF has yet to be explored.

The maintenance of mitochondrial equilibrium is closely related to managing cell senescence [23]. Mitochondria play critical roles in the generation of energy and the stability of metabolic processes within the cell [24]. The maintenance of mitochondrial quality control is achieved through the processes of mitochondrial biogenesis, the processes of mitochondrial dynamics (fusion and fission), and the process of mitophagy [25]. Mitochondrial biogenesis is the growth and division of mitochondria to expand their numbers, and this process is managed by distinct pathways like the mitochondrial biogenesis factors PPARγ coactivator-1α (PGC1α)/nuclear respiratory factor 1 (NRF1)/mitochondrial transcription factor A (TFAM) pathway [26]. AECs from PF are found to have inadequate mitochondrial biogenesis [27], which is thought to be the cause of their senescence [24]. However, the molecular mechanism behind this disruption of mitochondrial biogenesis remains unknown.

In this study, we initially observed that citrate^{mt} was accumulated in AECs exposed to BLM *in vivo* and *in vitro*. By co-inhibiting Idh3α and CIC with shRNA or inhibitors, citrate^{mt} accumulation and senescence were induced in murine AECs. The accumulated citrate^{mt} was found to impede mitochondrial biogenesis and induce senescence in AECs. The senescence-associated secretory phenotype (SASP) secreted from senescent AECs activated the proliferation and transdifferentiation of fibroblasts into myofibroblasts. These findings suggest that citrate^{mt} accumulation could be a potential target for protecting against PF by inducing senescence.

2. Materials and methods

2.1. Animals

All experiments involving animals were conducted in accordance with the regulations established by the National Institutes of Health. Adult male C57BL/6 J mice weighing 20 ± 2 g were procured from Hunan SJA Laboratory Animal Co., Ltd (Hunan, China). The animals were kept in a 12-dark/light cycle with unrestricted access to food and water [28].

2.2. Animal treatment

Mice were randomly divided into two groups for PF models: the control group ($n = 10$), which received an intratracheal injection of saline, and the BLM group ($n = 10$), which received an intratracheal injection of BLM (3 mg/kg, in 50 μL saline, Nippon Kayaku, Japan). On Day 21, all mice were euthanized, and the lungs were collected for further analysis.

Mice were randomly divided into two groups for the virus-silencing models: the Con-shRNA group ($n = 6$), which received an intratracheal injection of an empty adenoviral vector, and the SPC-Slc25a1-shRNA + SPC-Idh3α-shRNA group ($n = 6$), which received an intratracheal injection of Slc25a1 (1×10^8 PFU/20 g, Genechem, Shanghai, China) and Idh3α (1×10^8 PFU/20 g, Genechem) adenoviral knockdown vectors containing the AEC-specific promoter SPC. On Day 30, all mice were euthanized, and their lungs were harvested for further analysis. All procedures were conducted under anesthesia with an intraperitoneal injection of sodium pentobarbital (80 mg/kg).

2.3. Pulmonary histopathological analysis

10% formalin was used to fix the left lung tissue, which was then embedded in paraffin and cut into 5 μm thick sections. H&E staining was employed to observe the tissue morphology, while Masson and Sirius's red staining was used to evaluate the collagen deposition. The Ashcroft score was utilized for the semi-quantitative assessment of fibrotic changes.

2.4. Immunofluorescent staining

Lung tissue sections were deparaffinized, permeabilized with 0.01 M citrate buffer, and heated for antigen retrieval, then blocking endogenous peroxidase with 3% H_2O_2 at 37 °C for 10 min. The cell samples were washed with PBS thrice and fixed with 4% para-formaldehyde for 15 min. The sections or cells were blocked with 5% bovine serum albumin (BSA, Biofroxx, Guangzhou, China) for 1 h and then incubated with primary antibodies in 1% BSA at 4 °C overnight. The sections were washed thrice with PBST and incubated with secondary antibodies for 1 h at room temperature. After washing in PBST three times, the nuclei were counterstained with DAPI (Solarbio, Beijing, China) for 30 s. The fluorescence was detected by a fluorescence microscope (Nikon, Japan). All antibodies used in the study are listed in Table 1.

2.5. Cell culture

MLE12, a murine AEC cell line, was procured from the American Type Culture Collection (ATCC) and maintained in a humidified incubator at 37 °C and 5% CO_2 in DMEM/F12 medium (Gibco, USA) supplemented with 2% newborn calf serum (BCS, Gibco) [29]. The NIH3T3 murine fibroblast cell lines were procured from ATCC. These cells were cultured in DMEM medium (Gibco) with 10% newborn calf serum at 37 °C and 5% CO_2 [30].

2.6. Cell treatment

For AEC senescence models, two groups of MLE12 cells were established: the control and the BLM groups. Cells in the BLM group were exposed to 0.1 U/mL BLM (Aladdin, Shanghai, China) for 48 h. For the inhibitor models, MLE12 cells were planted into plates, then grouped into four groups: the control group, the CIC inhibitor group: cells were treated with 2 mM BTA (a CIC inhibitor, Sigma-Aldrich), the IDH3α inhibitor group: cells were treated with 100 μM TBT (IDH3 inhibitor, Aladdin), the CIC inhibitor + IDH3α inhibitor group: cells were treated with 2 mM CIC inhibitor and 100 μM IDH3α inhibitor. After 24 h, the cells were collected.

For the virus-silencing models, MLE12 cells were planted and grouped into two groups: the Con-shRNA group: cells were treated with empty vector virus, and the Slc25a1-shRNA + Idh3α-shRNA group: cells were infected with Slc25a1-shRNA lentivirus (multi-plicity of infection:100, Genechem) and Idh3α-shRNA lentivirus (multiplicity of infection: 100, Genechem). After 16 h of lentivirus treatment, the supernatant was removed and replaced with a complete medium for 80 h. When MLE12 cells were cultured for 96 h, the

Table 1
Antibody dilutions and sources used in Western blot and Immunofluorescence in this study.

Antibodies	Dilution ratio	Source
Primary antibodies for western blotting		
Rabbit-*anti*-IDH3α antibody	1:1500	Abcam
Rabbit-*anti*-CIC antibody	1:1500	Invitrogen
Rabbit-*anti*-p53 antibody	1:1500	Proteintech
Rabbit-*anti*-p21 antibody	1:1500	ABclonal
Rabbit-*anti*-γ-H2AX antibody	1:1500	Boster
Rabbit-*anti*-Collagen I antibody	1:1500	ABclonal
Rabbit-*anti*-α-SMA antibody	1:3000	SAB
Mouse-*anti*-PGC1α antibody	1:1500	Proteintech
Rabbit-*anti*-NRF1 antibody	1:1500	Proteintech
Rabbit-*anti*-TFAM antibody	1:1500	Proteintech
Rabbit-*anti*-Tom20 antibody	1:1500	Proteintech
Rabbit-*anti*-PCNA antibody	1:1500	Proteintech
Rabbit-*anti*-α-Tubulin antibody	1:10,000	Servicebio
Rabbit-*anti*-β-Tubulin antibody	1:5000	Servicebio
Secondary antibodies for western blotting		
Goat anti-Rabbit antibody	1:7500	SAB
Goat anti-mouse antibody	1:5000	SAB
Primary antibodies for Immunofluorescence		
Rabbit anti-surfactant protein C antibody	1:400	ABclonal
Mouse *anti*-p53 antibody	1:200	Abcam
Mouse *anti*-p21 antibody	1:400	Proteintech
Rabbit *anti*-IDH3α antibody	1:400	Abcam
Rabbit *anti*-CIC antibody	1:400	Invitrogen
Rabbit anti-Tom20 antibody	1:200	Proteintech
Mouse *anti*-E-cadherin antibody	1:250	Arigo
Rabbit anti-Collagen I/COL1A2 antibody	1:400	ABclonal
Rabbit *anti*-PCNA antibody	1:200	Proteintech
Secondary antibodies for Immunofluorescence		
Green-fluorescent FITC goat anti-rabbit IgG	1:500	ABclonal
Red-fluorescent TRITC goat anti-rabbit IgG	1:500	ABclonal
Green-fluorescent FITC goat anti-mouse IgG	1:500	ABclonal
Red-fluorescent TRITC goat anti-mouse IgG	1:500	ABclonal

supernatants containing SASP were collected as the conditioned medium (CM). The supernatant was centrifuged at 3000 rpm for 5 min, and the sediment was retained. NIH3T3 cells were planted into plates and treated with 10% supernatants containing SASP for 24 h.

2.7. Real-time quantitative polymerase chain reaction (RT-qPCR)

RT-qPCR was performed as in our previous study [31]. Total RNA was extracted from MLE12 or homogenized lung tissues using RNAiso Plus (Takara, Kusatsu, Japan). The concentration and quality of total RNA were evaluated by spectrophotometry (Thermo Fisher Scientific, USA). Total RNA was reverse-transcribed to cDNA utilizing a Reverse Transcription kit (Takara). Subsequently, RT-qPCR was carried out with TB Green PCR Master Mix (Takara) on a Bio-Rad real-time PCR system (CFX96 Touch™, Bio-Rad, USA). The mRNA levels were normalized in comparison to *β-actin* or *18S*. The fold change for each mRNA was calculated using the $2^{-\Delta\Delta Ct}$ method. All primer sequences are shown in Table 2.

2.8. Western blotting

MLE12, NIH3T3, and lung tissue lysates were prepared using a RIPA Lysis Buffer (Solarbio) that included a protease inhibitor, phenylmethanesulfonyl fluoride (PMSF, Solarbio), and a phosphatase inhibitor Cocktail (CWBIO, Jiangsu, China). The protein concentration was then determined using the BCA Protein Assay Kit (Thermo Fisher Scientific). 30 μg of total protein was separated on a 12% SDS-PAGE gel and then transferred onto a polyvinylidene difluoride (PVDF) membrane. The membranes were initially blocked with 5% non-fat milk or BSA at room temperature for 1 h and then probed with primary antibodies overnight at 4 °C. Following this, the membranes were washed four times with TBST and incubated with HRP-conjugated secondary antibodies for 1 h at room temperature. Subsequently, protein signals were detected using an ECL kit (CWBIO) and ChemiDoc XRS (Bio-Rad). The quantitative results of the Western blot were determined by Image Lab Analyzer software (Bio-Rad). The antibodies used in the study are detailed in Table 1.

2.9. Measurement of mitochondrial membrane potential (MMP)

Measurement of MMP was accomplished following the previously established protocol [32]. The JC-1 Assay Kit (Beyotime, Shanghai, China) was employed to measure the MMP of cells. After washing twice with PBS, the cells cultured in 48-well plates were incubated with JC-1 for 20 min at 37 °C in the dark. In healthy mitochondria, JC-1 aggregates to form a polymer in the mitochondrial matrix, emitting intense red fluorescence (Excitation, 585 nm; Emission, 590 nm). Conversely, in unhealthy mitochondria, due to the decline/loss of MMP, JC-1 monomers are present in the cytoplasm, resulting in green fluorescence (Excitation, 514 nm; Emission, 529 nm). Consequently, alterations in the ratio of red/green indicate a change in MMP.

2.10. Detection of intracellular ROS and mitochondrial ROS generation

DCFH-DA (Beyotime, Shanghai, China) and MitoSOX Red (MCE, USA) were used to measure the production of intracellular reactive oxygen species (ROS) and mitochondrial ROS. After treatment, MLE12 cells were incubated at 37 °C for 25 min with DCFH-DA (10 μM) or MitoSOX Red (500 nM) and washed with PBS three times. The cells were observed by fluorescence microscopy (Nikon, Japan).

2.11. MitoTracker staining assay

MLE12 cells were stained with MitoTracker Green (Yeasen Biotech, 40742ES50) according to the manufacturer's instructions. Images were obtained using fluorescence microscopy (Nikon, Japan).

Table 2
Sequences of the primer used in this study.

Gene	Forward 5′ to 3′	Reverse 5′ to 3′
m-*Collagen I*	GAGCGGAGAGTACTGGATCG	GCTTCTTTTCCTTGGGGTTC
m-*Collagen III*	GCACAGCAGTCCAACGTAGA	TCTCCAAATGGGATCTCTGG
m-*p16*	CTCTGCTCTTGGGATTGGC	GTGCGATATTTGCGTTCCG
m-*p21*	GTGAGGAGGAGCATGAATGGA	GAACAGGTCGGACATCACCA
m-*p53*	GCCCATGCTACAGAGGAGTC	AAGGCTTGGAAGGCTCTAGG
m-*Idh3α*	TTGCTGGTGGTGTTCAGACA	ATTGCTGTGACATTGCGCTC
m-*Slc25a1*	TGCAGCCAGTGTCTTTGGAA	AGGATCTTCAAGCCGCAGTC
m-*Tgf-β1*	ACTGGAGTTGTACGGCAGTG	GGGGCTGATCCCGTTGATTT
m-*Il-6*	TCCGGAGAGGAGACTTCACA	GTGACTCCAGCTTATCTCTTGGT
m-*Il-8*	TGCATGGACAGTCATCCACC	ATGACAGACCACAGAACGGC
m-*Il-1β*	CAGGCAGGCAGTATCACTCA	AGCTCATATGGGTCCGACAG
m-Mmp2	TCGCCCATCATCAAGTTCCC	CCTTGGGGCAGCCATAGAAA
m-*18s*	AAACGGCTACCACATCCAAG	CCTCCAATGGGATCCTCGTTA
m-*β-actin*	TTCCAGCCTTCCTTCTTG	GGAGCCAGAGCAGTAATC

2.12. Senescence-associated β-galactosidase (SA-β-gal) staining

SA-β-gal staining was performed as previously described [10]. The MLE12 cells on a dish were stained using the Senescence β-Galactosidase Staining Kit (Beyotime) as the manufacturer's instructions. Firstly, the live cells were washed twice with PBS and then fixed with 1*x* Fixation solution for 15 min at room temperature. Subsequently, they were rinsed twice with PBS and stained with β-Galactosidase Staining Solution for 2 h overnight at 37 °C in a dry incubator (no CO_2). The following day, the cell samples were observed, and pictures were captured using a microscope.

2.13. Cell growth assay

The cell growth assay was conducted following the previously established methodology [30]. Cell Counting Kit-8 (CCK-8, Dojindo Molecular Technologies, Japan) was used to assess cell viability. Cells were seeded into 96-well plates (1000 cells/well) and then, after 12 h of serum deprivation, were exposed to various concentrations of CM containing SASP for 24 h. Subsequently, 10 μL of CCK-8 was added to each well, and the plates were incubated at 37 °C for an additional 1 h. The absorbance was then measured at 450 nm using a
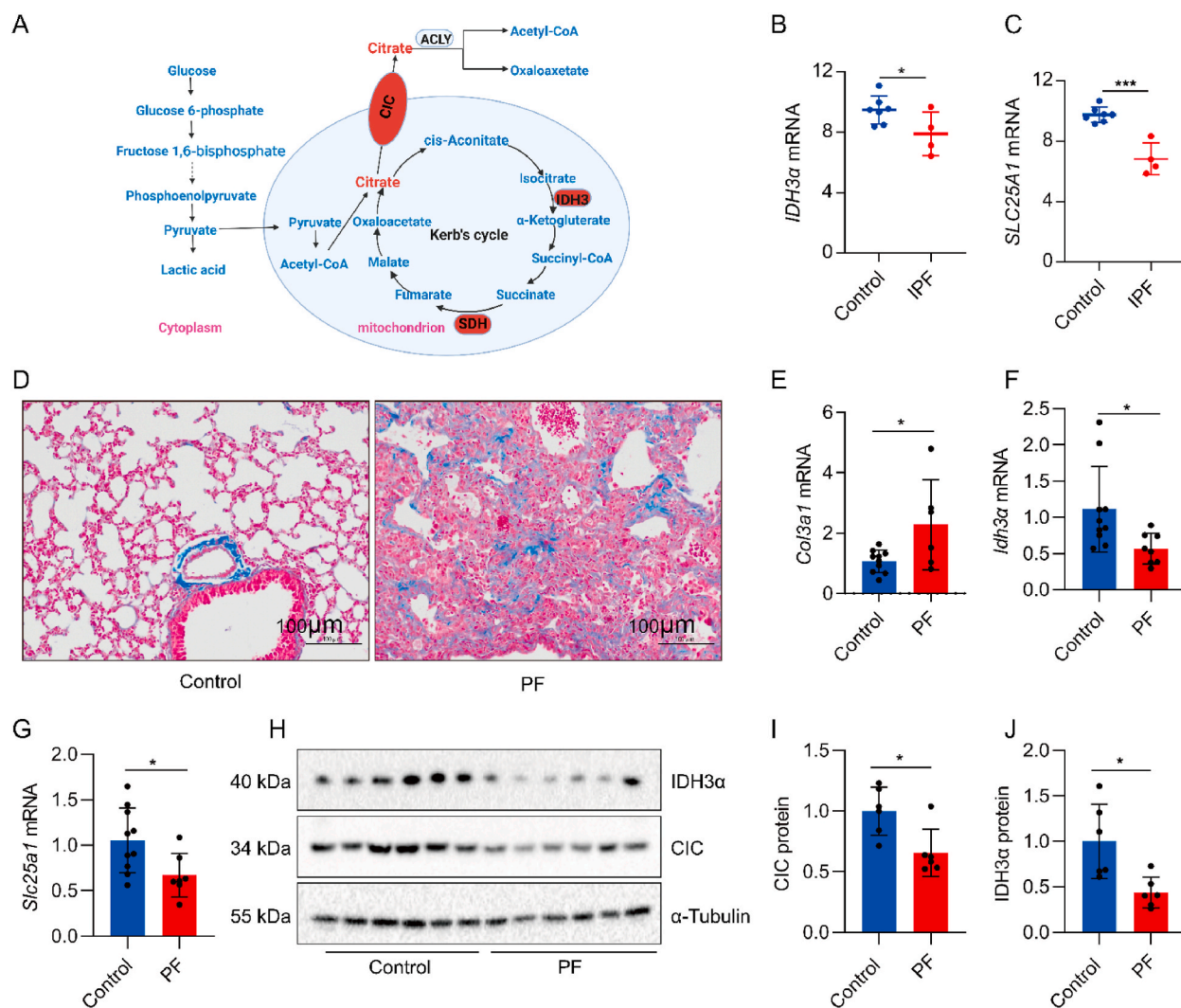

Fig. 1. IDH3α and CIC expression are down-regulated in the lungs of PF. (A) The pathway of citrate metabolism and transportation. (B–C) Human *IDH3α* and *SLC25A1* mRNA expression in the lung tissues from IPF subjects ($n = 4$) and controls ($n = 7$) were determined by microarray (GSE185691). C57BL/6 J mice received BLM (3 mg/kg, intratracheal injection) to establish a PF model. Mice were sacrificed on the 21st day after the BLM injection. (D) Lung histopathology was stained with Masson's trichrome (bar = 100 μm). (E) RT-qPCR results showed increased *Col3a1* mRNA on the 21st day after BLM administration ($n = 6$–10). (F–G) RT-qPCR results showed decreased Idh3α and Slc25a1 mRNA expressions on the 21st day after BLM administration ($n = 6$–10). (H–J) Western blot showed decreased IDH3α and CIC proteins on the 21st day after BLM administration ($n = 6$). Data are expressed as the mean ± SD. *$P < 0.05$.
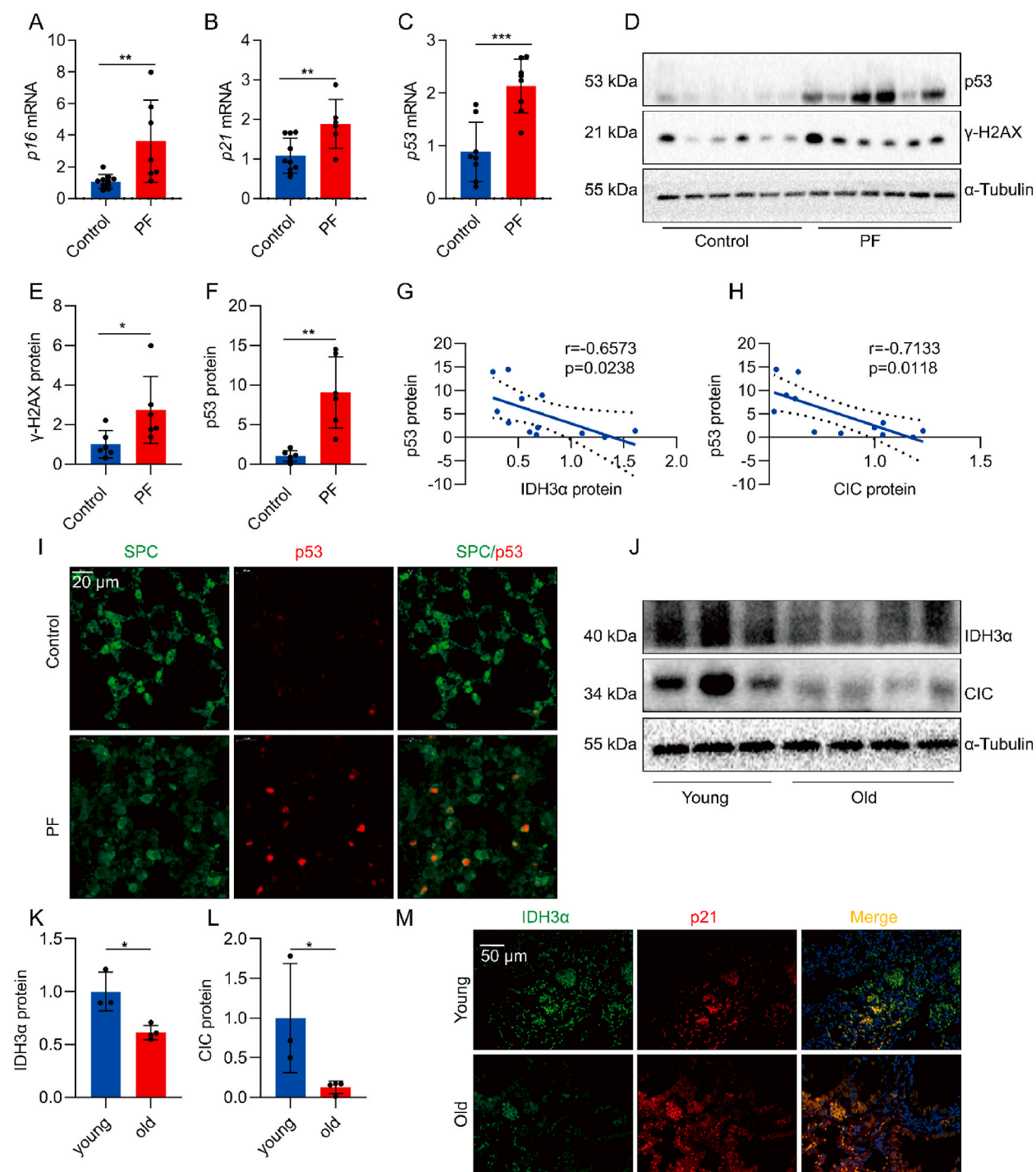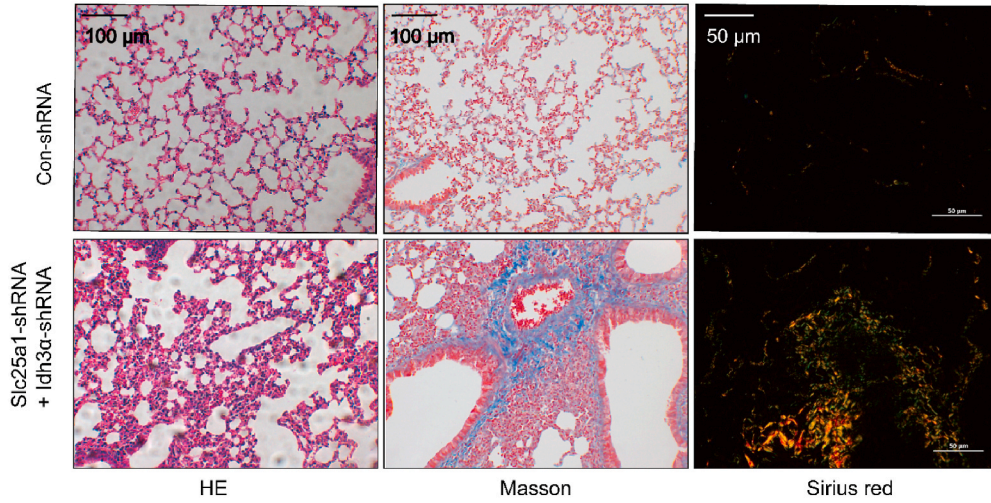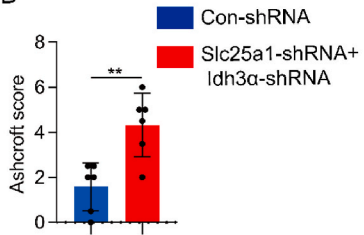
Fig. 2. Downregulation of IDH3α and CIC are positively related to lung aging. C57BL/6 J mice received BLM (3 mg/kg, intratracheal injection) to establish a PF model and were sacrificed on the 21st day after the BLM injection. (A–C) The mRNA expressions of *p16, p21,* and *p53* were detected by RT-qPCR ($n = 5$–10). (D–F) The protein expressions of p53 and γ-H2AX were detected by Western Blot. (G–H) The correlations of p53 with IDH3α and CIC were analyzed by GraphPad Prism 9. (I) The fluorescence intensity of SPC and p53 was detected by immunofluorescence (bar = 20 μm), green: SPC, red: p53. (J–L) The protein expressions of IDH3α and CIC were detected by Western Blot. (M) The fluorescence intensity of IDH3α and p21 were detected by immunofluorescence (bar = 50 μm), green: IDH3α, red: p21. Data are expressed as the mean ± SD. *$P < 0.05$, **$P < 0.01$, and ***$P < 0.001$.
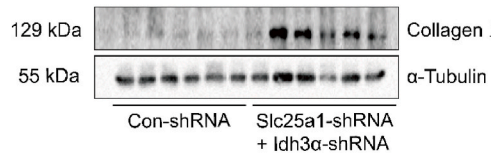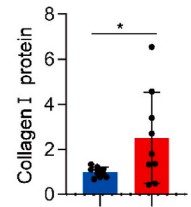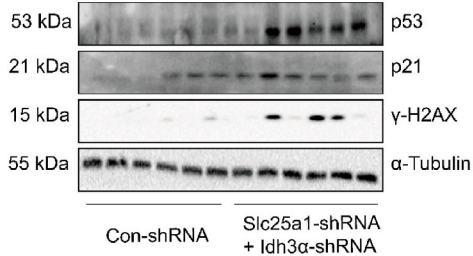
A

Con-shRNA
Slc25a1-shRNA
+ Idh3α-shRNA

HE   Masson   Sirius red

B

Ashcroft score

■ Con-shRNA
■ Slc25a1-shRNA+
  Idh3α-shRNA

**

C

129 kDa   Collagen Ⅰ
55 kDa   α-Tubulin

Con-shRNA   Slc25a1-shRNA
             + Idh3α-shRNA

D

Collagen Ⅰ protein

*

E

53 kDa   p53
21 kDa   p21
15 kDa   γ-H2AX
55 kDa   α-Tubulin

Con-shRNA   Slc25a1-shRNA
             + Idh3α-shRNA

F

p53 protein

**

G

p21 protein

*

H

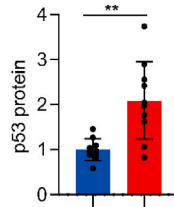γ-H2AX protein

*

I

Con-shRNA
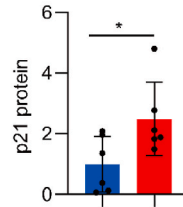Slc25a1-shRNA
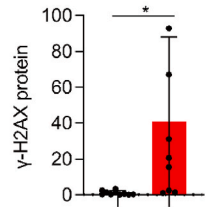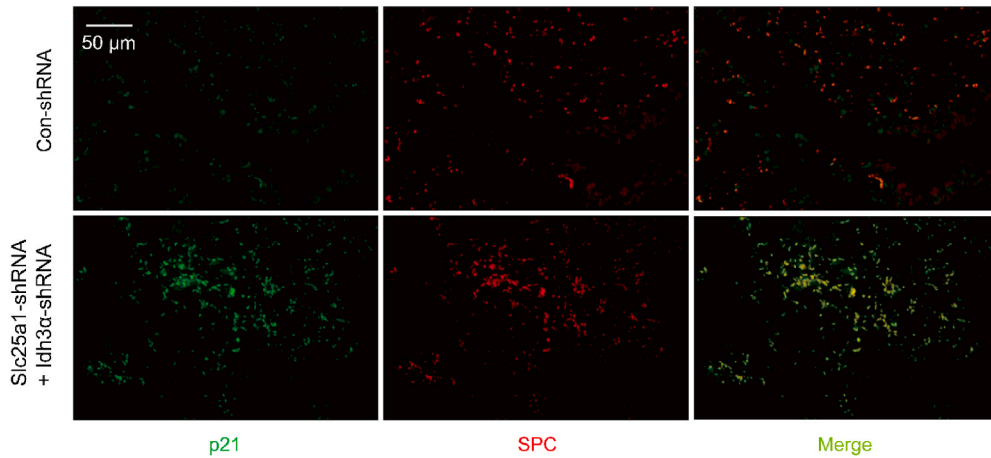+ Idh3α-shRNA

p21   SPC   Merge

(caption on next page)

Fig. 3. Silencing IDH3α and CIC leads to senescence and spontaneous fibrosis in the lungs. C57BL/6 J mice were intratracheally injected with SPC promoter-adenovirus silencing vectors for Idh3α and Slc25a1 (1×10^8 PFU/20 g) and survived to the 30th day. (A) Lung histopathology was performed with H&E (bar = 100 μm), Masson's trichrome (bar = 100 μm), and Sirius Red staining (bar = 50 μm) 30 days after the adenovirus injection. (B) The fibrosis score was evaluated independently by three blinded pathologists ($n = 6$). (C–D) The Collagen I protein expression was detected by Western blot ($n = 6$). (E–H) The protein expressions of p53, p21, and γ-H2AX were detected by Western Blot ($n = 6$). (I) The fluorescence intensity of SPC and p21 were detected by immunofluorescence (bar = 50 μm), green: p21, red: SPC. Data are expressed as the mean ± SD. *$P <$ 0.05 and **$P <$ 0.01.

UV spectrophotometer (Thermo Fisher Scientific).

2.14. Statistical analysis

Data were presented as mean ± SD and obtained from at least three independent experiments. Statistical analysis was conducted using GraphPad Prism 9 software (GraphPad Software, Inc., San Diego, CA, USA) or SPSS 26.0 (IBM). To determine the differences between the two groups, an unpaired two-tailed *t*-test was conducted. Correlations were then calculated using Spearman rank-order coefficients. Statistical comparisons among the multiple groups were assessed with ANOVA, and Tukey's test was used as a post hoc test for pairwise comparisons. The results were expressed as mean ± SD values and statistical significance was set at $P < 0.05$.

3. Results

3.1. Accumulation of citrate^mt occurs in the lungs of PF

Citrate^mt participates in the TCA cycle through the downstream key enzymes IDH3 and succinate dehydrogenase. And citrate^mt can be transported into the cytoplasm *via* CIC (Fig. 1A) [33]. First, microarray analysis of GSE185691 revealed a reduction in the *IDH3α* and *SLC25A1* mRNA levels in the lungs of IPF patients compared to those of healthy controls (Fig. 1B and C). Next, we investigated the change of CIC and IDH3α in the PF lung tissue. Compared with the control group, the mice in the PF group showed infiltration of inflammatory cells, thickening of alveolar septa, and fibrous scar (Fig. 1D). The expression of *Col3a1* mRNA was up-regulated in the lungs of BLM-induced PF mice (Fig. 1E). These were consistent with previously published findings [34]. Further, we detected the mRNA and protein expression of IDH3α and CIC in the lungs. We found that the expressions of IDH3α and CIC in the lungs were down-regulated under the BLM challenge (Fig. 1F–J). Collectively, these data indicate that citrate^mt accumulation occurs in the lungs of PF.

### 3.2. Citrate^mt accumulation is positively related to lung aging

Next, we investigated the role of citrate^mt accumulation in PF. The mRNA expressions of senescence-related molecules *p16*, *p21*, and *p53* were significantly increased (Fig. 2A–C). We also found that the protein expressions of p53 and γ-H2AX were significantly up-regulated in the lungs of PF mice (Fig. 2D–F). Immunofluorescent staining showed that the increased fluorescence intensity of p53 overlapped with surfactant protein C (SPC) (Fig. 2I), indicating the senescence of AECs during PF. Interestingly , not only IDH3α protein expression negatively correlated with the p53 protein in the lungs of PF mice (Fig. 2G), but also CIC protein expression negatively correlated with the p53 protein (Fig. 2H). Aging is an essential feature in PF patients [1]. We found that the expressions of IDH3α and CIC protein were decreased in the lungs of old mice compared with young mice (Fig. 2J-L). IDH3α protein expression was negatively correlated with the p21 protein in the lung tissues of old mice (Fig. 2M). Altogether, these results demonstrate that citrate^mt accumulation is positively related to lung aging.

3.3. AECs-specific citrate^mt accumulation leads to senescence and spontaneous fibrosis in the lungs

To further clarify the effect of citrate^mt accumulation in AECs during fibrosis and aging, we injected SPC promoter-adenovirus silencing vectors for Idh3α (Idh3α-shRNA) and Slc25a1 (Slc25a1-shRNA) (1×10^8 PFU/20 g) to establish AEC-specific citrate^mt accumulation mice model as our previous study [22]. Immunofluorescence staining showed co-localization of *E*-cadherin and IDH3α or CIC was decreased in AECs-specifically silencing Idh3α and Slc25a1 group, suggesting that AEC-specific citrate^mt accumulation occurred (Fig. S1). In pathological morphology, mice receiving AEC-specific Idh3α-shRNA and Slc25a1-shRNA treatment showed apparent inflammatory cell infiltration, alveolar wall thickness, and fiber foci formation in the lungs (Fig. 3A). Remarkably, silencing AECs-specific IDH3α and CIC increased lung fibrosis scores (Fig. 3B) and up-regulated the protein expression of collagenI in the lungs (Fig. 3C and D). These results suggest that AECs-specific citrate^mt accumulation triggers spontaneous PF. Interestingly, we found that p53, p21, and γ-H2AX protein expressions were increased in the lungs of mice receiving AEC-specific Idh3α shRNA and Slc25a1 shRNA treatment (Fig. 3E–H). And senescence marker p21 was co-localized with SPC (Fig. 3I). Collectively, these data suggest that AECs-specific citrate^mt accumulation leads to senescence and spontaneous fibrosis in mice lungs.

3.4. Citrate^mt accumulation drives senescence of AECs in vitro

Senescent AECs drive PF by exhausting the alveolar regenerative potential and triggering pathological remodeling [35]. To
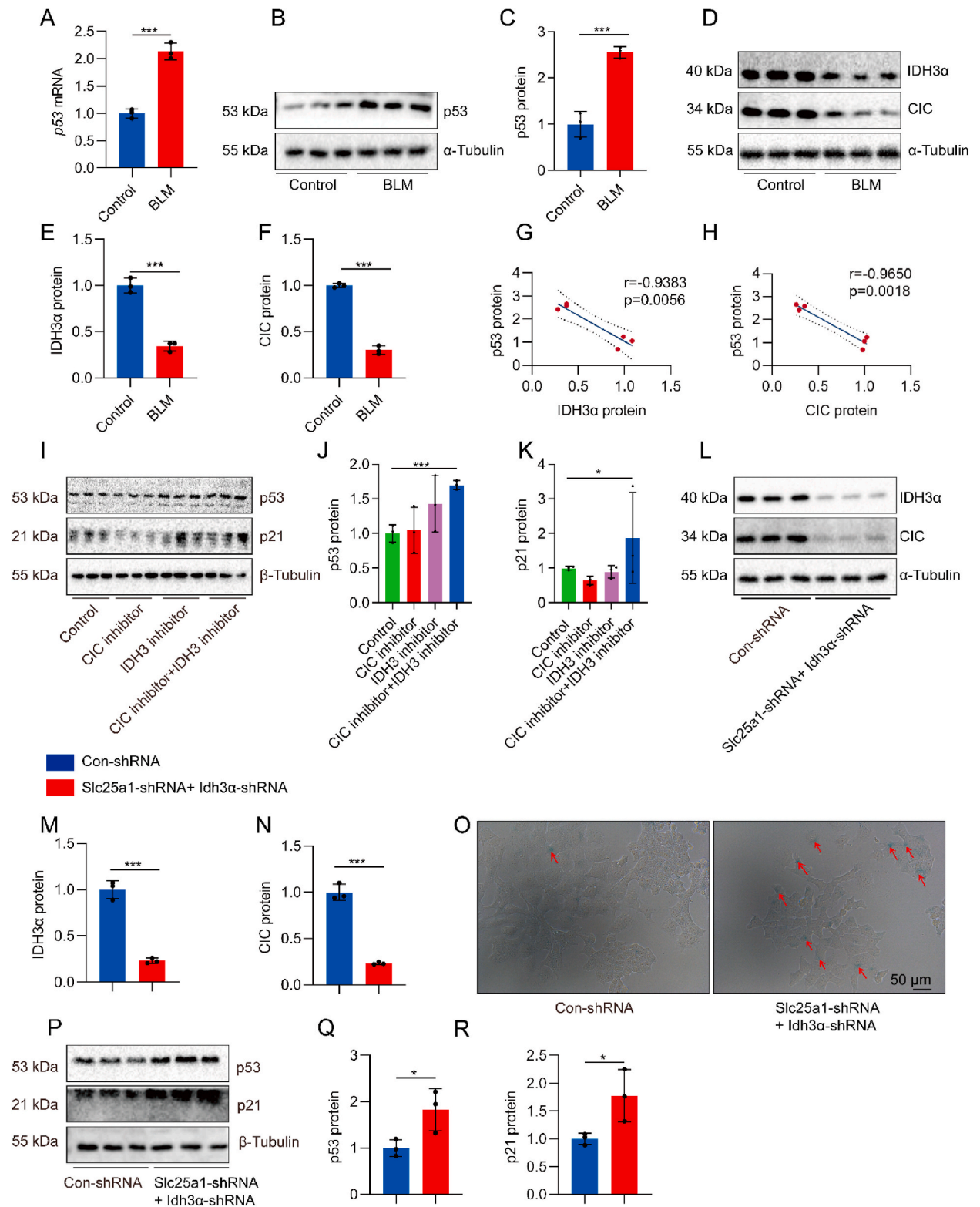
(caption on next page)

Fig. 4. Silencing IDH3α and CIC drives the senescence of AECs *in vitro*. MLE12 cells were treated with BLM (0.01 U/mL) for 48 h. (A–C) The p53 level was measured by RT-qPCR and Western Blot ($n = 3$). (D–F) The protein expressions of IDH3α and CIC were measured by Western Blot ($n = 3$). (G–H) The correlations of p53 with IDH3α and CIC were analyzed by GraphPad Prism 9. (I–K) MLE12 cells were treated with IDH3α inhibitor (100 μM) and CIC inhibitor (2 mM) for 24 h, and the levels of p53 and p21 proteins were detected by Western Blot ($n = 3$). MLE12 cells were treated with Idh3α-shRNA and Slc25a1-shRNA for 96 h. (L–N) The protein expressions of IDH3α and CIC were detected by Western Blot ($n = 3$). (O) Senescence was confirmed by SA-β-gal staining (bar = 50 μm). (P–R) The protein expressions of p53 and p21 were detected by Western Blot ($n = 3$). Data are expressed as the mean ± SD. *$P < 0.05$, **$P < 0.01$, and ***$P < 0.001$.

illustrate the role of citrate[mt] accumulation in AECs senescence, we first investigated whether citrate[mt] accumulation occurred in senescent AECs *in vitro*. Murine AECs MLE12 were treated with BLM (0.01 U/mL) for 48 h. We found that BLM up-regulated the p53 mRNA and protein expressions while down-regulated the IDH3α and CIC protein expressions (Fig. 4A–F). And the levels of IDH3α and CIC were negatively correlated with the p53 protein (Fig. 4G and H). Next, we established a citrate[mt] accumulation model with Idh3α-shRNA and Slc25a1-shRNA (Fig. 4L − N), which could induce citrate[mt] accumulation reported in our previous study [22]. We found that citrate[mt] accumulation increased the intensity of SA-β-gal staining positive (Fig. 4O) and significantly elevated the expression of p53 and p21 (Fig. 4P-R). Citrate[mt] accumulation also significantly decreased the level of proliferating cell nuclear antigen (PCNA) in MLE12 cells (Fig. S2). In addition, we pretreated MLE12 with IDH3 and CIC inhibitors (BTA and TBT). Compared with the control group, MLE12 cells receiving BTA and TBT exerted higher senescence-related protein levels (Fig. 4I-K). Overall, these data indicate that citrate[mt] accumulation drives the senescence of AECs *in vitro*.

3.5. Citrate[mt] accumulation impairs the mitochondrial biogenesis of AECs

Mitochondrial dysfunction has been widely implicated in PF [27]. Mitochondrial membrane potential (MMP), an index of mitochondrial bioenergetics, was impaired in MLE12 cells with citrate[mt] accumulation (Fig. 5A). Citrate[mt] accumulation was also seen to significantly promote the creation of intracellular and mitochondrial ROS (Fig. 5B), indicating the mitochondrial dysfunction of AECs. Mitochondrial biogenesis plays a crucial role in producing new healthy mitochondria [25]. *In vitro*, we found that citrate[mt] accumulation reduced the levels of mitochondrial biogenesis factors: TOM20, PGC1α, TFAM, and NRF1 in MLE12 cells (Fig. 5D–H). The mitochondrial number was much lower after citrate[mt] accumulation than the control group (Fig. 5C). *In vivo*, citrate[mt] accumulation also decreased the expressions of PGC1α and TFAM in mice lungs (Fig. 5I–K). These data suggest that citrate[mt] accumulation damages the mitochondrial biogenesis of AECs, which may contribute to AEC senescence.

3.6. Citrate[mt] accumulation-triggered AECs senescence derives fibroblast proliferation and transdifferentiation via SASP
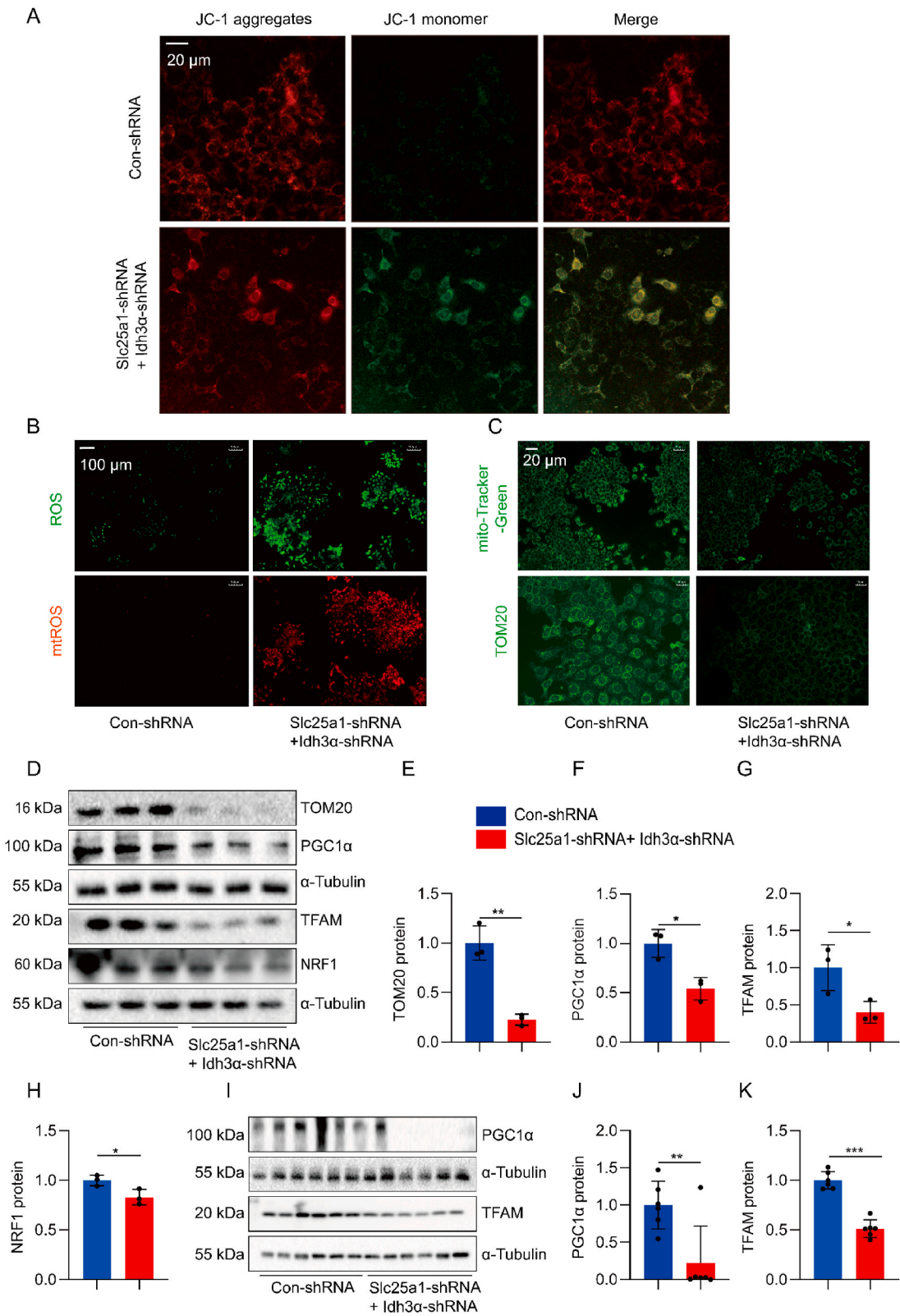
Senescent AECs release a considerable amount of SASP, such as transforming growth factors and cytokines, which stimulate the proliferation and transdifferentiation of neighboring lung fibroblasts, thus hastening the progression of PF [10,30]. To evaluate the effects of CM derived from AECs with citrate[mt] accumulation on fibrosis*in vitro*, we employed an embryonic mouse fibroblast cell line (NIH3T3). MLE12 cells were treated with Slc25a1-shRNA and Idh3α-shRNA, and the cell culture supernatant was collected as CM (Fig. 6A and B). The CCK8 assay demonstrated that 10% CM had a marked effect on increasing cell viability in NIH3T3 cells compared to the control group (Fig. 6C). Besides, fibroblast activation markers (collagen I and α-SMA) were increased after exposure to 10% CM in NIH3T3 cells (Fig. 6D–F). Those findings indicate that citrate[mt] accumulation triggers AECs senescence, thus inducing fibroblast proliferation and transdifferentiation *via* SASP.

4. Discussion

In this study, we identified a novel role of citrate[mt] accumulation in regulating the senescence of AECs and its potential mechanism on BLM-induced PF *in vivo* and *in vitro*. Mechanistically, citrate[mt] accumulation impaired mitochondrial biogenesis, triggering senescence of AECs. Furthermore, SASP secreted by senescent AECs induced the proliferation and differentiation of lung fibroblasts, thus accelerating the process of PF (Fig. 7). Taken together, these data suggest that citrate[mt] accumulation is involved in AEC senescence during PF.

Aging drives PF characterized by the mass secretion of profibrotic factors and lung parenchyma and interstitium destruction, leading to poor respiratory function and life quality [5,11]. Emerging evidence has revealed that the senescence of AECs drives PF through both consuming alveolar regeneration potential and SASP-induced pathological remodeling. Therefore, pharmacological manipulation of AECs' senescence signaling is a reasonable therapeutic strategy for PF. Our previous studies have found that COX-2/sEH dual inhibitor PTUPB alleviates the BLM-induced PF by inhibiting AEC senescence [10]. Blocking triggering receptor expressed on myeloid cells-1, an inflammatory receptor, relieves AEC senescence, rescuing PF outcomes [11]. Herein, we identified citrate[mt] accumulation as a senescent stimulus in PF.

Glucose metabolism is an indispensable life process, supplying cells and organisms with energy and materials [36,37]. Metabolic enzymes and their metabolites in the TCA cycle are related to aging [38–40]. For example, inhibition of IDH1 could induce ovarian cancer cell senescence and thus inhibit tumor cell growth [21]. Fumarate hydratase (FH) is a key enzyme in the TCA cycle, which can convert fumarate into malic acid. FH^{+/-} rat primary fibroblasts exhibited anti-aging properties [41]. Pyruvate produced by glycolysis can be converted into citrate after entering the mitochondria, which participates in Krebs through IDH3. Alternatively, it can be transported to the cytoplasm *via* CIC on the mitochondrial surface to produce acetyl-CoA and oxaloacetate under the action of ACLY

A   JC-1 aggregates   JC-1 monomer   Merge

Con-shRNA

Slc25a1-shRNA + Idh3α-shRNA

B

ROS

mtROS

Con-shRNA   Slc25a1-shRNA +Idh3α-shRNA

C

mito-Tracker -Green

TOM20

Con-shRNA   Slc25a1-shRNA +Idh3α-shRNA

D

16 kDa   TOM20
100 kDa   PGC1α
55 kDa   α-Tubulin
20 kDa   TFAM
60 kDa   NRF1
55 kDa   α-Tubulin

Con-shRNA   Slc25a1-shRNA + Idh3α-shRNA

E   TOM20 protein   **

F   PGC1α protein   *

G   TFAM protein   *

Con-shRNA
Slc25a1-shRNA+ Idh3α-shRNA

H   NRF1 protein   *

I
100 kDa   PGC1α
55 kDa   α-Tubulin
20 kDa   TFAM
55 kDa   α-Tubulin

Con-shRNA   Slc25a1-shRNA + Idh3α-shRNA

J   PGC1α protein   **

K   TFAM protein   ***

(caption on next page)

Fig. 5. Silencing IDH3α and CIC damages the mitochondrial biogenesis in AECs. MLE12 cells were treated with Idh3α-shRNA and Slc25a1-shRNA for 96 h. (A) Representative images of MLE12 cells loaded with the mitochondrial membrane potential indicator JC-1 (bar = 20 μm). (B) Intracellular ROS were measured by DCFH-DA staining and the mitochondrial ROS were determined by MitoSOX staining (bar = 100 μm). (C) MitoTracker Green staining and immunofluorescence of TOM20 determined the mitochondrial number (bar = 20 μm). (D–H) The levels of Tom20, PGC1α, TFAM, and NRF1 were detected by Western Blot ($n = 3$). C57BL/6 J mice were intratracheally injected with SPC promoter-adenovirus silencing vectors for Idh3α and Slc25a1 (1×10^8 PFU/20 g) and survived to the 30th day. (I–K) The protein expressions of TFAM and PGC1α were detected by Western Blot ($n = 6$). Data are expressed as the mean ± SD. *$P < 0.05$, **$P < 0.01$, and ***$P < 0.001$.
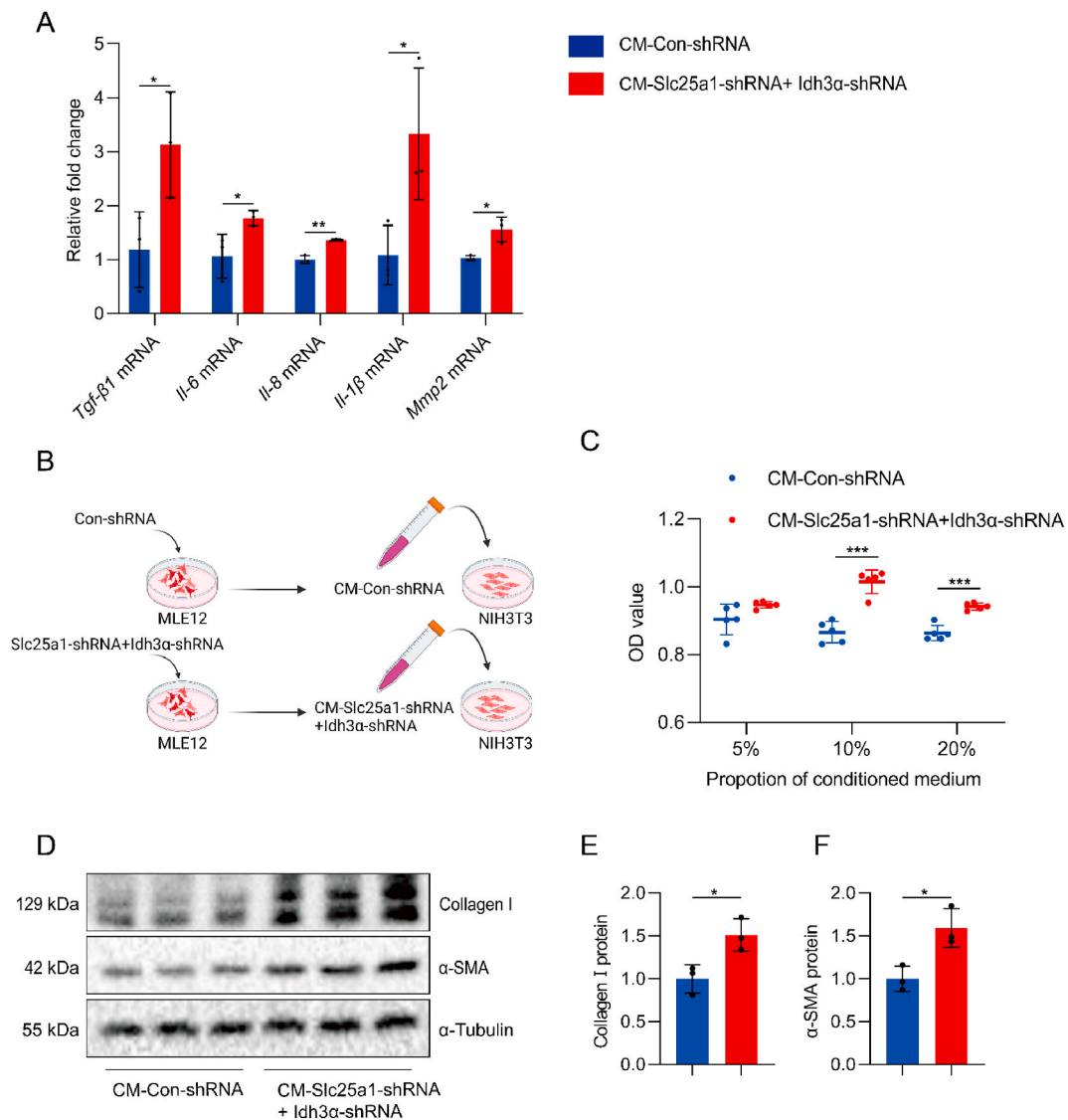

Fig. 6. Silencing IDH3α and CIC triggers AECs senescence and induces fibroblast proliferation and transdifferentiation *via* SASP. MLE12 cells were treated with Idh3α-shRNA and Slc25a1-shRNA for 96 h. (A) The mRNA expressions of *Tgf-β1, Il-6, Il-8,Il-1β* and *Mmp2* were detected by RT-qPCR ($n = 3$). (B) The protocol for conditioned medium experimentation. MLE12 cells were treated with Idh3α-shRNA and Slc25a1-shRNA for 96 h, and cell culture supernatant was collected as CM. Fibroblasts were starved (without serum) for 12 h and then treated with different concentrations of CM for 24 h. (C) CCK8 assay assessed the results of different groups at 5%, 10%, and 20% of CM on NIH3T3 cell viability ($n = 3$). (D–F) The protein expressions of collagen I and α-SMA were detected by Western Blot ($n = 3$). Data are expressed as the mean ± SD. *$P < 0.05$ and ***$P < 0.001$.

[42,43]. IDH3 and CIC are highly related to citrate[mt] homeostasis. Decreased levels of IDH3 and CIC suggest an accumulation of citrate[mt] [22]. Our prior investigation revealed that citrate[mt] accumulation occurred and facilitated necroptosis of AECs in lipopolysaccharide-induced ALI mice [22]. Promisingly, we found that mice with AECs-specific Idh3α and Slc25a1 deficiency
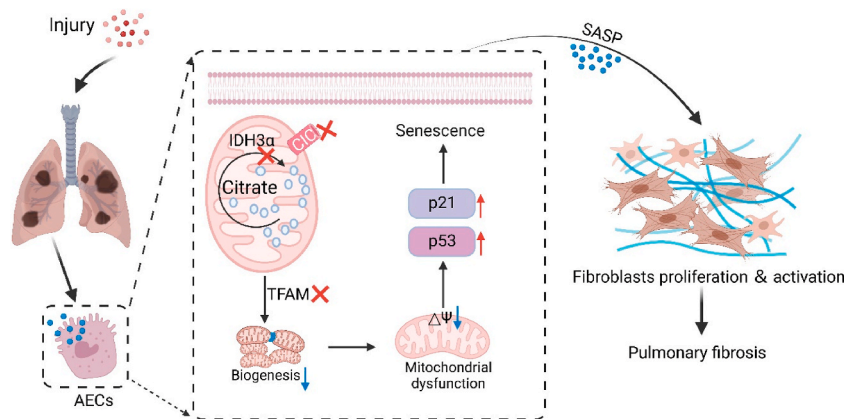
Fig. 7. Schematic representation of the proposed mechanisms for citrate^mt accumulation-induced AECs senescence during PF. Citrate^mt accumulation triggers AECs senescence during BLM-induced PF by impairing mitochondrial biogenesis.

exhibited inflammatory cell infiltration, fiber foci formation, down-regulation of SPC, and up-regulation of aging-related proteins in the lungs of mice. Moreover, *in vitro*, AECs with citrate^mt accumulation showed senescent characteristics, with high expression of aging-related proteins and increased SA-β-gal activity. AECs are structural cells in the lungs, and injured AECs affect gas exchange, which is a significant reason for dyspnea in PF patients [44]. Various damage factors stimulate AECs and destroy the alveolar epithelial integrity, thus exacerbating PF. SPC is one of the specific markers of AECs, and its decrease can increase alveolar surface tension and aggravate AECs injury. Consequently, these data support that citrate^mt accumulation induces AEC injury *via* senescence.

Mitochondria act as a central hub in the mammalian cell. Its homeostasis and precise function are critical for cell fitness and survival [27]. The maintenance of mitochondrial mass is achieved *via* mitochondrial biogenesis, mitochondrial dynamics, and mitophagy [45]. Mitochondrial biogenesis is essential for regulating newborn mitochondria to guarantee cell energy metabolism [46]. It mainly involves the replication of mitochondrial DNA (mtDNA), the synthesis of mtDNA-encoded proteins, and the coordination of mitochondrial dynamics. PGC1α, as a major co-transcription factor, translocates to the nucleus and binds to NRF1/2, transcriptionally activating the expression of TFAM. This process drives mtDNA transcription and replication [47,48]. Mitochondrial biogenesis deficiency is an early marker of mitochondrial damage, which leads to decreased ATP synthesis and oxidative stress, and ultimately cell senescence [49]. For example, PGC1α deficiency reduces proliferation of vascular smooth muscle cells, while simultaneously increasing the level of ROS and senescence [50]. Here, our findings indicate that AECs with accumulated citrate^mt had reduced expression of Tom20, PGC1α, TFAM, and NRF1 proteins. In addition, accumulated citrate^mt increased ROS and mitochondrial ROS generation, as well as decreased MMP in AECs, which are key signs of mitochondrial dysfunction [32]. Moreover, mice with AECs-specific Idh3α and Slc25a1 deficiency showed down-regulated levels of TFAM and PGC1α. These results suggest that increased citrate^mt accumulation harms mitochondrial biogenesis and reduces MMP of AECs, thus intensifying the senescence of AECs.

Emerging evidence has demonstrated that senescent AECs can promote the proliferation and differentiation of lung fibroblasts through the secretion of growth factors and cytokines as part of the SASP, thus accelerating the process of PF [35]. In this study, we found that the conditioned medium from AECs with citrate^mt accumulation significantly stimulated fibroblast proliferation and activation. Collectively, we speculate that mitochondrial citrate^mt accumulation impairs mitochondrial function, triggering AEC senescence, thus exacerbating lung fibrosis. To some extent, our study also reveals a novel mechanism underlying the initiation of cellular senescence in AECs: citrate^mt accumulation.

The limitations of this study are: i) In addition to senescence, apoptosis and necroptosis of AECs are also important causes of AEC loss in PF. While it is still unclear whether apoptosis (or necroptosis) occurs upon citrate accumulation in AECs during PF. ii) Besides measuring CIC and Idh3α protein levels, the direct citrate content in BLM-induced AECs or the mice lungs has to be detected in future studies. iii) Our study suggested decreased mRNA levels of IDH3α and SLC25A1 in IPF patients compared to healthy. Further studies using clinical patient specimens will be necessary to demonstrate the clinical significance of the increased citrate in IPF pathogenesis.

In conclusion, this is the first report revealing that citrate^mt accumulation contributes to the senescence of AECs during PF by mediating mitochondrial dysfunction. Therefore, targeting citrate^mt accumulation could be a potential strategy to reduce AEC senescence in PF patients. Our findings indicate that citrate^mt accumulation is an intrinsic pathogenic mechanism of PF.

Author contribution statement

Funding statement

Data availability statement

Data will be made available on request.

Declaration of competing interest

The authors declare that they have no known competing financial interests or personal relationships that could have appeared to influence the work reported in this paper.

Abbreviations

ACLY   ATP-dependent ATP citrate lyase
AECs   alveolar epithelial cells
BLM   Bleomycin
CM   conditioned medium
CIC   citrate carrier
FH   fumarate hydratase
IDH3   isocitrate dehydrogenase 3
mtDNA   mitochondrial DNA
MMP   mitochondrial membrane potential
TFAM   mitochondrial transcription factor A
NRF1   nuclear respiratory factor 1
PF   pulmonary fibrosis
PGC1α   PPARγ coactivator-1α
PCNA   proliferating cell nuclear antigen
ROS   reactive oxygen species
SASP   senescence-associated secretory phenotype
SA-β-gal   senescence-associated β-galactosidase
SPC   surfactant protein C
TCA cycle   tricarboxylic acid cycle

Appendix A. Supplementary data

Supplementary data to this article can be found online at https://doi.org/10.1016/j.heliyon.2023.e17361.

References

[1] S.J. Cho, H.W. Stout-Delgado, Aging and lung disease, Annu. Rev. Physiol. 82 (2020) 433–459, https://doi.org/10.1146/annurev-physiol-021119-034610.

[2] G. Raghu, M. Remy-Jardin, L. Richeldi, C.C. Thomson, Y. Inoue, T. Johkoh, M. Kreuter, D.A. Lynch, T.M. Maher, F.J. Martinez, M. Molina-Molina, J.L. Myers, A. G. Nicholson, C.J. Ryerson, M.E. Strek, L.K. Troy, M. Wijsenbeek, M.J. Mammen, T. Hossain, B.D. Bissell, D.D. Herman, S.M. Hon, F. Kheir, Y.H. Khor, M. Macrea, K.M. Antoniou, D. Bouros, I. Buendia-Roldan, F. Caro, B. Crestani, L. Ho, J. Morisset, A.L. Olson, A. Podolanczuk, V. Poletti, M. Selman, T. Ewing, S. Jones, S.L. Knight, M. Ghazipura, K.C. Wilson, Idiopathic pulmonary fibrosis (an update) and progressive pulmonary fibrosis in adults: an official ATS/ERS/ JRS/ALAT clinical practice guideline, Am. J. Respir. Crit. Care Med. 205 (2022) e18–e47, https://doi.org/10.1164/rccm.202202-0399ST.

[3] J. Behr, A. Prasse, M. Kreuter, J. Johow, K.F. Rabe, F. Bonella, R. Bonnet, C. Grohe, M. Held, H. Wilkens, P. Hammerl, D. Koschel, S. Blaas, H. Wirtz, J.H. Ficker, W. Neumeister, N. Schonfeld, M. Claussen, N. Kneidinger, M. Frankenberger, S. Hummler, N. Kahn, S. Tello, J. Freise, T. Welte, P. Neuser, A. Gunther, R. investigators, Pirfenidone in patients with progressive fibrotic interstitial lung diseases other than idiopathic pulmonary fibrosis (RELIEF): a double-blind, randomised, placebo-controlled, phase 2b trial, Lancet Respir. Med. 9 (2021) 476–486, https://doi.org/10.1016/S2213-2600(20)30554-3.

[4] Y. Umemura, Y. Mitsuyama, K. Minami, T. Nishida, A. Watanabe, N. Okada, K. Yamakawa, K. Nochioka, S. Fujimi, Efficacy and safety of nintedanib for pulmonary fibrosis in severe pneumonia induced by COVID-19: an interventional study, Int. J. Infect. Dis. 108 (2021) 454–460, https://doi.org/10.1016/j. ijid.2021.05.055.

[5] P. Spagnolo, J.A. Kropski, M.G. Jones, J.S. Lee, G. Rossi, T. Karampitsakos, T.M. Maher, A. Tzouvelekis, C.J. Ryerson, Idiopathic pulmonary fibrosis: disease mechanisms and drug development, Pharmacol. Ther. 222 (2021), 107798, https://doi.org/10.1016/j.pharmthera.2020.107798.

[6] P.M. George, C.M. Patterson, A.K. Reed, M. Thillai, Lung transplantation for idiopathic pulmonary fibrosis, Lancet Respir. Med. 7 (2019) 271–282, https://doi.org/10.1016/S2213-2600(18)30502-2.

[7] F.J. Martinez, H.R. Collard, A. Pardo, G. Raghu, L. Richeldi, M. Selman, J.J. Swigris, H. Taniguchi, A.U. Wells, Idiopathic pulmonary fibrosis, Nat. Rev. Dis. Prim. 3 (2017), 17074, https://doi.org/10.1038/nrdp.2017.74.

[8] M.J. Schafer, T.A. White, K. Iijima, A.J. Haak, G. Ligresti, E.J. Atkinson, A.L. Oberg, J. Birch, H. Salmonowicz, Y. Zhu, D.L. Mazula, R.W. Brooks, H. Fuhrmann-Stroissnigg, T. Pirtskhalava, Y.S. Prakash, T. Tchkonia, P.D. Robbins, M.C. Aubry, J.F. Passos, J.L. Kirkland, D.J. Tschumperlin, H. Kita, N.K. LeBrasseur, Cellular senescence mediates fibrotic pulmonary disease, Nat. Commun. 8 (2017), 14532, https://doi.org/10.1038/ncomms14532.

[9] M. Korfei, B. MacKenzie, S. Meiners, The ageing lung under stress, Eur. Respir. Rev. 29 (2020), https://doi.org/10.1183/16000617.0126-2020.

[10] C.Y. Zhang, J.X. Duan, H.H. Yang, C.C. Sun, W.J. Zhong, J.H. Tao, X.X. Guan, H.L. Jiang, B.D. Hammock, S.H. Hwang, Y. Zhou, C.X. Guan, COX-2/sEH dual inhibitor PTUPB alleviates bleomycin-induced pulmonary fibrosis in mice via inhibiting senescence, FEBS J. 287 (2020) 1666–1680, https://doi.org/10.1111/febs.15105.

[11] J.B. Xiong, J.X. Duan, N. Jiang, C.Y. Zhang, W.J. Zhong, J.T. Yang, Y.B. Liu, F. Su, Y. Zhou, D. Li, H.H. Yang, C.X. Guan, TREM-1 exacerbates bleomycin-induced pulmonary fibrosis by aggravating alveolar epithelial cell senescence in mice, Int. Immunopharm. 113 (2022), 109339, https://doi.org/10.1016/j.intimp.2022.109339.

[12] C. Yao, X. Guan, G. Carraro, T. Parimon, X. Liu, G. Huang, A. Mulay, H.J. Soukiasian, G. David, S.S. Weigt, J.A. Belperio, P. Chen, D. Jiang, P.W. Noble, B.R. Stripp, Senescence of alveolar Type 2 cells drives progressive pulmonary fibrosis, Am. J. Respir. Crit. Care Med. 203 (2021) 707–717, https://doi.org/10.1164/rccm.202004-1274OC.

[13] Q. Wang, L. Duan, X. Li, Y. Wang, W. Guo, F. Guan, S. Ma, Glucose metabolism, neural cell senescence and alzheimer's disease, Int. J. Mol. Sci. 23 (2022), https://doi.org/10.3390/ijms23084351.

[14] A. Poff, A.P. Koutnik, K.M. Egan, S. Sahebjam, D. D'Agostino, N.B. Kumar, Targeting the Warburg effect for cancer treatment: ketogenic diets for management of glioma, Semin. Cancer Biol. 56 (2019) 135–148, https://doi.org/10.1016/j.semcancer.2017.12.011.

[15] F. Hariton, M. Xue, N. Rabbani, M. Fowler, P.J. Thornalley, Sulforaphane delays fibroblast senescence by curbing cellular glucose uptake, increased glycolysis, and oxidative damage, Oxid. Med. Cell. Longev. 2018 (2018), 5642148, https://doi.org/10.1155/2018/5642148.

[16] B.A. Olenchock, M.G. Vander Heiden, Pyruvate as a pivot point for oncogene-induced senescence, Cell 153 (2013) 1429–1430, https://doi.org/10.1016/j.cell.2013.06.001.

[17] P. Strzyz, Alternative cycle for citrate, Nat. Rev. Mol. Cell Biol. 23 (2022) 305, https://doi.org/10.1038/s41580-022-00475-w.

[18] J.G. Leandro, J.M. Espindola-Netto, M.C. Vianna, L.S. Gomez, T.M. DeMaria, M.M. Marinho-Carvalho, P. Zancan, H.A. Paula Neto, M. Sola-Penna, Exogenous citrate impairs glucose tolerance and promotes visceral adipose tissue inflammation in mice, Br. J. Nutr. 115 (2016) 967–973, https://doi.org/10.1017/S0007114516000027.

[19] L. Fontana, S.E. Mitchell, B. Wang, V. Tosti, T. van Vliet, N. Veronese, B. Bertozzi, D.S. Early, P. Maissan, J.R. Speakman, M. Demaria, The effects of graded caloric restriction: XII. Comparison of mouse to human impact on cellular senescence in the colon, Aging Cell 17 (2018), e12746, https://doi.org/10.1111/acel.12746.

[20] Y. Zhao, X. Liu, F. Si, L. Huang, A. Gao, W. Lin, D.F. Hoft, Q. Shao, G. Peng, Citrate promotes excessive lipid biosynthesis and senescence in tumor cells for tumor therapy, Adv. Sci. 9 (2022), e2101553, https://doi.org/10.1002/advs.202101553.

[21] E.S. Dahl, R. Buj, K.E. Leon, J.M. Newell, Y. Imamura, B.G. Bitler, N.W. Snyder, K.M. Aird, Targeting IDH1 as a prosenescent therapy in high-grade serous ovarian cancer, Mol. Cancer Res. 17 (2019) 1710–1720, https://doi.org/10.1158/1541-7786.MCR-18-1233.

[22] H.H. Yang, H.L. Jiang, J.H. Tao, C.Y. Zhang, J.B. Xiong, J.T. Yang, Y.B. Liu, W.J. Zhong, X.X. Guan, J.X. Duan, Y.F. Zhang, S.K. Liu, J.X. Jiang, Y. Zhou, C.X. Guan, Mitochondrial citrate accumulation drives alveolar epithelial cell necroptosis in lipopolysaccharide-induced acute lung injury, Exp. Mol. Med. 54 (2022) 2077–2091, https://doi.org/10.1038/s12276-022-00889-8.

[23] S. Miwa, S. Kashyap, E. Chini, T. von Zglinicki, Mitochondrial dysfunction in cell senescence and aging, J. Clin. Invest. 132 (2022), https://doi.org/10.1172/JCI158447.

[24] B.J. Moss, S.W. Ryter, I.O. Rosas, Pathogenic mechanisms underlying idiopathic pulmonary fibrosis, Annu. Rev. Pathol. 17 (2022) 515–546, https://doi.org/10.1146/annurev-pathol-042320-030240.

[25] J.L. Larson-Casey, C. He, A.B. Carter, Mitochondrial quality control in pulmonary fibrosis, Redox Biol. 33 (2020), 101426, https://doi.org/10.1016/j.redox.2020.101426.

[26] L.D. Popov, Mitochondrial biogenesis: an update, J. Cell Mol. Med. 24 (2020) 4892–4899, https://doi.org/10.1111/jcmm.15194.

[27] M. Bueno, J. Calyeca, M. Rojas, A.L. Mora, Mitochondria dysfunction and metabolic reprogramming as drivers of idiopathic pulmonary fibrosis, Redox Biol. 33 (2020), 101509, https://doi.org/10.1016/j.redox.2020.101509.

[28] W.J. Zhong, H.H. Yang, X.X. Guan, J.B. Xiong, C.C. Sun, C.Y. Zhang, X.Q. Luo, Y.F. Zhang, J. Zhang, J.X. Duan, Y. Zhou, C.X. Guan, Inhibition of glycolysis alleviates lipopolysaccharide-induced acute lung injury in a mouse model, J. Cell. Physiol. 234 (2019) 4641–4654, https://doi.org/10.1002/jcp.27261.

[29] H.H. Yang, J.X. Duan, S.K. Liu, J.B. Xiong, X.X. Guan, W.J. Zhong, C.C. Sun, C.Y. Zhang, X.Q. Luo, Y.F. Zhang, P. Chen, B.D. Hammock, S.H. Hwang, J.X. Jiang, Y. Zhou, C.X. Guan, A COX-2/sEH dual inhibitor PTUPB alleviates lipopolysaccharide-induced acute lung injury in mice by inhibiting NLRP3 inflammasome activation, Theranostics 10 (2020) 4749–4761, https://doi.org/10.7150/thno.43108.

[30] J.H. Tao, T. Liu, C.Y. Zhang, C. Zu, H.H. Yang, Y.B. Liu, J.T. Yang, Y. Zhou, C.X. Guan, Epoxyeicosatrienoic acids inhibit the activation of murine fibroblasts by blocking the TGF-beta1-smad2/3 signaling in a PPARgamma-dependent manner, Oxid. Med. Cell. Longev. 2022 (2022), 7265486, https://doi.org/10.1155/2022/7265486.

[31] W.J. Zhong, T. Liu, H.H. Yang, J.X. Duan, J.T. Yang, X.X. Guan, J.B. Xiong, Y.F. Zhang, C.Y. Zhang, Y. Zhou, C.X. Guan, TREM-1 governs NLRP3 inflammasome activation of macrophages by firing up glycolysis in acute lung injury, Int. J. Biol. Sci. 19 (2023) 242–257, https://doi.org/10.7150/ijbs.77304.

[32] H.L. Jiang, H.H. Yang, Y.B. Liu, C.Y. Zhang, W.J. Zhong, X.X. Guan, L. Jin, J.R. Hong, J.T. Yang, X.H. Tan, Q. Li, Y. Zhou, C.X. Guan, L-OPA1 deficiency aggravates necroptosis of alveolar epithelial cells through impairing mitochondrial function during acute lung injury in mice, J. Cell. Physiol. 237 (2022) 3030–3043, https://doi.org/10.1002/jcp.30766.

[33] I. Martínez-Reyes, N.S. Chandel, Mitochondrial TCA cycle metabolites control physiology and disease, Nat. Commun. 11 (2020) 102, https://doi.org/10.1038/s41467-019-13668-3.

[34] D. Cheng, Q. Xu, Y. Wang, G. Li, W. Sun, D. Ma, S. Zhou, Y. Liu, L. Han, C. Ni, Metformin attenuates silica-induced pulmonary fibrosis via AMPK signaling, J. Transl. Med. 19 (2021) 349, https://doi.org/10.1186/s12967-021-03036-5.

[35] H. Cui, N. Xie, S. Banerjee, T. Dey, R.M. Liu, V.B. Antony, Y.Y. Sanders, T.S. Adams, J.L. Gomez, V.J. Thannickal, N. Kaminski, G. Liu, CD38 mediates lung fibrosis by promoting alveolar epithelial cell aging, Am. J. Respir. Crit. Care Med. 206 (2022) 459–475, https://doi.org/10.1164/rccm.202109-2151OC.

[36] Z. Li, H. Zhang, Reprogramming of glucose, fatty acid and amino acid metabolism for cancer progression, Cell. Mol. Life Sci. 73 (2016) 377–392, https://doi.org/10.1007/s00018-015-2070-4.

[37] P. Vaupel, G. Multhoff, Revisiting the Warburg effect: historical dogma versus current understanding, J. Physiol. 599 (2021) 1745–1757, https://doi.org/10.1113/JP278810.

[38] W. Zhu, X. Chen, G. Guo, H. Liu, R. Ma, Y. Wang, Y. Liang, Y. Sun, M. Wang, R. Zhao, P. Gao, Low glucose-induced overexpression of HOXC-AS3 promotes metabolic reprogramming of breast cancer, Cancer Res. 82 (2022) 805–818, https://doi.org/10.1158/0008-5472.Can-21-1179.

[39] B. Hu, M. Yu, X. Ma, J. Sun, C. Liu, C. Wang, S. Wu, P. Fu, Z. Yang, Y. He, Y. Zhu, C. Huang, X. Yang, Y. Shi, S. Qiu, H. Sun, A.X. Zhu, J. Zhou, Y. Xu, D. Zhu, J. Fan, IFNalpha potentiates anti-PD-1 efficacy by remodeling glucose metabolism in the hepatocellular carcinoma microenvironment, Cancer Discov. 12 (2022) 1718–1741, https://doi.org/10.1158/2159-8290.CD-21-1022.

[40] R. Han, J. Liang, B. Zhou, Glucose metabolic dysfunction in neurodegenerative diseases-new mechanistic insights and the potential of hypoxia as a prospective therapy targeting metabolic reprogramming, Int. J. Mol. Sci. 22 (2021), https://doi.org/10.3390/ijms22115887.

[41] Z. Fan, L. Li, X. Li, M. Zhang, M. Dou, J. Zhao, J. Cao, X. Deng, M. Zhang, H. Li, Z. Suo, Anti-senescence role of heterozygous fumarate hydratase gene knockout in rat lung fibroblasts in vitro, Aging (Albany NY) 11 (2019) 573–589, https://doi.org/10.18632/aging.101761.

[42] C. Lussey-Lepoutre, K.E. Hollinshead, C. Ludwig, M. Menara, A. Morin, L.J. Castro-Vega, S.J. Parker, M. Janin, C. Martinelli, C. Ottolenghi, C. Metallo, A. P. Gimenez-Roqueplo, J. Favier, D.A. Tennant, Loss of succinate dehydrogenase activity results in dependency on pyruvate carboxylation for cellular anabolism, Nat. Commun. 6 (2015) 8784, https://doi.org/10.1038/ncomms9784.

[43] M.T. Doan, M.A. Teitell, Krebs and an alternative TCA cycle, Cell Res. 32 (2022) 509–510, https://doi.org/10.1038/s41422-022-00664-4.

[44] A. Kumar, B. Abdelmalak, Y. Inoue, D.A. Culver, Pulmonary alveolar proteinosis in adults: pathophysiology and clinical approach, Lancet Respir. Med. 6 (2018) 554–565, https://doi.org/10.1016/S2213-2600(18)30043-2.

[45] M.A. Eldeeb, R.A. Thomas, M.A. Ragheb, A. Fallahi, E.A. Fon, Mitochondrial quality control in health and in Parkinson's disease, Physiol. Rev. 102 (2022) 1721–1755, https://doi.org/10.1152/physrev.00041.2021.

[46] C.F. Bennett, P. Latorre-Muro, P. Puigserver, Mechanisms of mitochondrial respiratory adaptation, Nat. Rev. Mol. Cell Biol. 23 (2022) 817–835, https://doi.org/10.1038/s41580-022-00506-6.

[47] M. Zhao, Y. Wang, L. Li, S. Liu, C. Wang, Y. Yuan, G. Yang, Y. Chen, J. Cheng, Y. Lu, J. Liu, Mitochondrial ROS promote mitochondrial dysfunction and inflammation in ischemic acute kidney injury by disrupting TFAM-mediated mtDNA maintenance, Theranostics 11 (2021) 1845–1863, https://doi.org/10.7150/thno.50905.

[48] J.H. Hwang, K.M. Kim, H.T. Oh, G.D. Yoo, M.G. Jeong, H. Lee, J. Park, K. Jeong, Y.K. Kim, Y.G. Ko, E.S. Hwang, J.H. Hong, TAZ links exercise to mitochondrial biogenesis via mitochondrial transcription factor A, Nat. Commun. 13 (2022) 653, https://doi.org/10.1038/s41467-022-28247-2.

[49] C. Lefranc, M. Friederich-Persson, F. Foufelle, A. Nguyen Dinh Cat, F. Jaisser, Adipocyte-mineralocorticoid receptor alters mitochondrial quality control leading to mitochondrial dysfunction and senescence of visceral adipose tissue, Int. J. Mol. Sci. 22 (2021), https://doi.org/10.3390/ijms22062881.

[50] G. Salazar, A. Cullen, J. Huang, Y. Zhao, A. Serino, L. Hilenski, N. Patrushev, F. Forouzandeh, H.S. Hwang, SQSTM1/p62 and PPARGC1A/PGC-1alpha at the interface of autophagy and vascular senescence, Autophagy 16 (2020) 1092–1110, https://doi.org/10.1080/15548627.2019.1659612.